Monocarboxylate transporter antagonism reveals metabolic vulnerabilities of viral-driven lymphomas

Emmanuela N. Bonglack[1,2], Joshua E. Messinger[3], Jana M. Cable[2], K. Mark Parnell[4], James Ch'ng[5], Heather R. Christofk[6], and Micah A. Luftig[2#].

[1]Department of Pharmacology and Cancer Biology, Duke University School of Medicine, Durham, NC, 27710

[2]Department of Molecular Genetics and Microbiology, Duke Center for Virology, Duke University School of Medicine, Durham, NC, 27710

[3]Active Motif, Inc., 1914 Palomar Oaks Way # 150, Carlsbad, CA 92008

[4]Vettore, LLC, San Francisco, CA, 94158

[5]Department of Pediatrics, Division of Hematology/Oncology, David Geffen School of Medicine at UCLA, Los Angeles, CA, 90095

[6]Department of Biological Chemistry, David Geffen School of Medicine at UCLA, Los Angeles, CA, 90095

#Corresponding author: Micah A. Luftig

Micah.luftig@duke.edu

Phone: 919-668-3091

ABSTRACT

Epstein-Barr Virus (EBV) is a ubiquitous herpesvirus that typically causes asymptomatic infection but can promote B lymphoid tumors in the immune-suppressed. *In vitro,* EBV infection of primary B cells stimulates glycolysis during immortalization into lymphoblastoid cell lines (LCLs). Lactate export during glycolysis is crucial for continued proliferation of many cancer cells-part of a phenomenon known as the “Warburg effect,” and is mediated by the monocarboxylate transporters 1 and 4 (MCT1 and MCT4). However, the role of MCT1/4 has yet to be studied in EBV-associated malignancies which display Warburg-like metabolism *in vitro*. Here, we show that EBV infection of B lymphocytes directly promotes temporal induction of MCT1 and MCT4 through the viral proteins EBNA2 and LMP1 respectively, with MCT1 being induced early after infection and MCT4 late. Remarkably, singular MCT1 inhibition early, and dual MCT1/4 inhibition in LCLs using a novel MCT4-selective inhibitor led to growth arrest and lactate buildup. Metabolic profiling in LCLs revealed significatly reduced oxygen consumption rates (OCR) and NAD+/NADH ratios, contrary to prevous observations of increased OCR and unaltered NAD+/NADH ratios in MCT1/MCT4-inhibited cancer cells. Furthermore, U-^{13}C6 glucose labeling of MCT1/4-inhibited LCLs also revealed increased labeling of glutathione in the presence of elevated ROS and depleted glutathione pools, as well as increased labeling of *de novo* pyrimidine biosynthetic intermediates, suggesting broad effects on LCL metabolism. These vulnerabilities sensitized LCLs as well as EBV+, and the related gammaherpesvirus KSHV+ lymphoma cell lines to killing by metformin and phenformin, pointing at a novel therapeutic approach for viral lymphomas.

38 **INTRODUCTION**

39 Epstein-Barr Virus (EBV) is a ubiquitous human herpesvirus transmitted through saliva,
40 with more than 95% of the world being infected by adulthood. Primary EBV infection is typically
41 asymptomatic and surmounts to latency establishment in quiescent memory B cells in the
42 peripheral blood(1). However, in immunocompromised persons, EBV reactivation can cause
43 uncontrolled latent EBV-induced B-cell proliferation and frank lymphoma. Recent evidence
44 suggests that host responses such as the DNA damage response (DDR) and metabolic stress
45 play a significant cell-intrinsic role in preventing EBV-driven B-cell transformation(2, 3).

46 EBV infection of primary human peripheral blood B cells *in vitro* produces indefinitely
47 proliferating lymphoblastoid cell lines (LCLs). LCLs express the Latency III growth program, where
48 all six EBV Nuclear Antigens, or EBNAs, (EBNA-LP, 1, 2, 3A, 3B, and 3C) and two Latent
49 Membrane Proteins, or LMPs, (LMP1 and LMP2A/B) are present. This gene expression program
50 mimics that of many EBV-associated B-lymphoid cancers, making LCLs a suitable model for
51 studying mechanisms underlying tumorigenesis(4). Prior to Latency III establishment in LCLs and
52 shortly after EBV infection of B cells, a transient period of hyperproliferation, called Latency IIb, is
53 induced, where only the viral EBNAs are expressed in the absence of the LMPs(5, 6). This
54 culminates in an irreversible growth arrest in most cells caused by a persistent DNA Damage
55 Response (DDR)(7). However, a very small subset (<10%) of hyperproliferating cells evade host
56 barriers like the DDR, and transition into Latency III-expressing LCLs within weeks(2).

57 During EBV immortalization of B cells into LCLs, increased energetic demands for
58 continued proliferation drive an upregulation of glycolysis and extracellular acidification rates
59 (ECAR)(3, 8–10). While the ECAR is largely a reflection of lactate export into the extracellular
60 environment, the magnitude and role of lactate export during EBV-driven B-cell immortalization
61 remains poorly characterized. Besides being a glycolytic waste product, lactate has recently
62 emerged to play a key role in tumor development, growth, and metastasis(11, 12). Furthermore,
63 intracellular lactate buildup can have dire consequences on cell homeostasis due to acidification

64 by lactic acid, highlighting the importance of lactate export for sustained cell growth and
65 survival(13).

66 Proton-coupled lactate export is driven by the plasma membrane proteins
67 monocarboxylate transporters 1 and 4 (MCT1 and MCT4). MCT1 has a much higher affinity for
68 lactate than MCT4, making it the primary lactate transporter under normal physiological conditions
69 (14–16). MCT4, however, is typically expressed in highly glycolytic tissues, or when intracellular
70 lactate concentrations are high, such as during aerobic glycolysis(17–19). MCT1 and MCT4 have
71 the ability to transport other monocarboxylates such as pyruvate and ketone bodies like
72 acetoacetate and β-hydroxybutyrate(15, 19, 20). However, these transporters are most commonly
73 associated with their role in lactate transport across the plasma membrane, especially during
74 tumor development, growth, and metastasis(21–23). As such, MCT1 and MCT4 act as essential
75 buffers at the intersection of the intracellular and extracellular environments, sensing
76 monocarboxylate concentrations and facilitating rapid transport based on the needs of the
77 cell(24–26). Not surprisingly, MCT1 and MCT4 are commonly expressed in a wide variety of
78 tumors, exporting lactate from glycolytic cancer cells, which can later be recycled by oxidative
79 cells in the tumor microenvironment(27, 28).

80 Targeting MCT1 and MCT4-mediated lactate export has become a highly attractive
81 therapeutic strategy in recent years, as blocking lactate export can lead to cell cycle arrest, and
82 sensitize tumor cells to killing by other metabolic inhibitors(20, 22, 29, 30). MCT1 inhibitors are
83 currently in Phase I clinical trials for a number of solid tumors and lymphomas(31). While these
84 inhibitors have proven to effectively reduce tumor burden in preclinical models of MCT1-
85 overexpressing cancers, they are unfortunately ineffective in MCT1/MCT4-co-expressing cancers
86 due to the redundant role of MCT4 as a lactate exporter(32). This highlights the need for MCT4-
87 specific inhibitors, which are unfortunately not commercially available to date. Furthermore, while
88 inhibition of MCT1 and MCT4 universally leads to a buildup of intracellular lactate in tumor cells,
89 the mechanisms underlying growth arrest and cell death are not fully understood. Thus, studying

90 how MCT1 and MCT4 are regulated in diverse contexts is critical for expanding our understanding
91 of their role not only in tumorigenesis, but cell biology and homeostasis at large.
92 Given their established roles in tumor development both *in vitro* and *in vivo*, we reasoned
93 that MCT1 and MCT4-mediated lactate export might contribute to EBV-mediated B-cell
94 tumorigenesis, and virus-associated lymphoma cell growth more broadly. To address this, we
95 measured changes in lactate concentration and MCT expression through EBV-mediated B-cell
96 outgrowth and perturbed MCT1 and MCT4 function with small molecule antagonists. Our data
97 identify metabolic vulnerabilities that we propose could be exploited for the treatment of viral-
98 associated cancers.
99
100 **RESULTS**
101 **EBV infection of human B cells leads to an increase in lactate accumulation, secretion,**
102 **and the lactate transporter MCT1.** We and others have previously demonstrated that EBV
103 infection of primary human B cells leads to upregulation of glycolysis as evidenced by an increase
104 in glycolytic enzymes and the extracellular acidification rate (ECAR)(3, 10). To determine whether
105 the increase in ECAR was indicative of an increase in lactate export from infected cells, we
106 harvested media from EBV-infected primary human B cells at several time points following
107 infection and measured media lactate. We found that media lactate levels increased steadily after
108 infection as cell proliferation initiated by day 4 and through long-term outgrowth (day 35 =
109 lymphoblastoid cell line, or LCL) (**Fig. 1A**). However, we did not observe a concomitant rise in
110 intracellular lactate until late times post infection (**Fig. 1B**). This finding led us to assess the
111 mechanism of lactate secretion during early infection.
112 Under normal physiological conditions in most cells, lactate transport is mediated by the
113 monocarboxylate transporter 1 (MCT1). We found that while resting B cells had little MCT1
114 expressed at the RNA or protein level, by day 7 EBV-infected B cells were expressing high levels
115 of MCT1 that persisted through LCL outgrowth (**Fig. 1C-D**). MCT1 is a known transcriptional target

116 of c-Myc, which is transcriptionally regulated upon EBV infection by the latency protein EBV
117 Nuclear Antigen 2 (EBNA2)(33). To test the hypothesis that EBNA2 is the viral protein responsible
118 for MCT1 induction, we utilized the P493-6 model of regulated EBNA2 expression(34). In this
119 system, an endogenous EBNA2 is regulated post-translationally by β-estradiol due to its fusion to
120 the estrogen receptor. Loss of EBNA2 in this system in the absence of β-estradiol led to a loss
121 of MCT1 as well as c-Myc mRNA and protein and the mRNA of two other EBNA2 and c-Myc
122 targets, HES1 and MTHFD2 (**Fig. 1E-I**) (10, 35). Similarly, turning EBNA2 back on in these cells
123 led to re-expression of these targets.
124
125 **MCT1 inhibition causes growth arrest and increased lactate in early EBV-infected B cells.**
126 The induction of MCT1 expression early after EBV infection led us to ask whether MCT1 was
127 crucial for maintaining EBV-infected B-cell proliferation or survival given the known detrimental
128 consequences of lactate accumulation(13). To assess this, we used the MCT1 inhibitor,
129 AZD3965, which is currently in clinical trials for MCT1-overexpressing lymphomas(31). We
130 treated EBV-infected peripheral blood mononuclear cells (PBMCs) concurrent with infection and
131 assessed CD19+ B-cell proliferation by flow cytometry using the proliferation tracking dye
132 CellTrace Violet at different days post infection. We found that treatment with AZD3965 led to a
133 dose-dependent decrease in B-cell proliferation on days 4 and 7 post EBV infection, accompanied
134 by an increase in intracellular lactate levels (**Fig. 2A-C**). This effect on proliferation was due to a
135 G1/S phase growth arrest and not to increased B-cell death (**Supp. 1**). However, this effect was
136 lost by 14 days post infection and later in immortalized LCLs, suggesting an acquired resistance
137 to MCT1 inhibition (**Fig. 2D-E**).
138
139 **EBV-infected B cells acquire resistance to MCT1 inhibition during B-cell transformation**
140 **through induction of MCT4.** Given the fact that our data indicate a significant increase in
141 intracellular lactate concentrations in LCLs compared to early-infected B cells, we hypothesized

142 that EBV immortalization might induce the expression of another lactate exporter, which would
143 mitigate the effects of MCT1 inhibition. We found that expression of the MCT1 family member,
144 MCT4, significantly increased between days 7 and day 14 post-EBV infection (**Fig. 3A-C**).
145 Interestingly, this time period correlates with a known switch in the EBV latency gene expression
146 program from latency IIb (EBNAs only - EBNA1, 2, 3A, 3B, 3C, and LP) to latency III (EBNAs and
147 LMPs – LMP1, LMP2A/B). Indeed, LMP1 expression within LCLs correlated with MCT4, but not
148 MCT1 or MCT2 expression (**Fig. 3D**). Furthermore, MCT4 was found to be upregulated by LMP1
149 in a publicly available RNA-Seq dataset of LMP1-expressing DG75, EBV-negative Burkitt
150 lymphoma cells (**Fig. 3E**). Thus, the switch to latency III and expression of the viral protein LMP1
151 leads to B-cell induction of MCT4 that may help compensate for elevated glycolysis in EBV-
152 infected cells as they progress to become LCLs.
153
154 **Dual MCT1/4 inhibition suppresses LCL growth and sensitizes to killing by ETC inhibitors.**
155 The unique expression profile of MCT1 with MCT4 at later stages of EBV-mediated B-cell
156 outgrowth along with the significant accumulation of lactate in LCLs, led us to hypothesize that
157 MCT4 might play a critical role in LCL growth. To assess the role of MCT4 in LCLs, we took
158 advantage of a novel, low-nanomolar MCT4 inhibitor, VB124, which displays >1,000-fold
159 selectivity over MCT1(36). Much to our surprise, MCT4 inhibition had no observed effect on LCL
160 growth or viability (**Fig. 4A**). However, we reasoned that though MCT4 expression was unique to
161 LCLs during EBV-mediated B-cell outgrowth, perhaps the presence of MCT1 in LCLs rendered
162 them resistant to singular MCT4 inhibition. To test this, we treated LCLs with both AZD3965 (1
163 μM) and VB124 (20 μM) and monitored cell proliferation. Dual inhibition of MCT1 and MCT4 led
164 to a significant decrease in LCL growth, accompanied by a four-fold increase in intracellular
165 lactate (**Fig. 4B, C**). Similar to the MCT1 inhibition effect on early-infected B-cell proliferation,
166 MCT1/4 combined inhibition led to growth arrest in LCLs rather than cell death (**Supp. Fig 2**).

167 Treatment with exogenous L-lactate phenocopied dual MCT1/4 inhibition suggests a direct role
168 for lactate accumulation in the regulation of EBV-immortalized LCL growth (**Supp. Fig 3**).
169 We next sought to assess whether MCT inhibition might also render LCLs susceptible to
170 arrest or killing by electron transport chain (ETC) inhibitors as this therapeutic strategy has been
171 successful in other cancer models(30, 37). Indeed, LCLs were 20-fold more susceptible to the
172 complex I inhibitor phenformin (IC_{50} from ~100μM to ~5μM) when coupled with growth inhibitory
173 concentrations of AZD3965 (1μM) and VB124 (20 μM) (**Fig. 4D**). Moreover, treatment of LCLs
174 with 10 μM phenformin induced significantly more cell death in MCT1/4-inhibited cells than alone
175 (**Fig. 4E**). This increased cell death was accompanied by increased intracellular lactate levels as
176 well (**Fig. 4F**). Finally, we found that MCT1/4 inhibition also sensitized LCLs to killing by the FDA-
177 approved ETC inhibitor, metformin (**Fig. 4G-H**). These experiments support our hypothesis that
178 lactate accumulation in EBV-infected cells renders them hyper-sensitive to the ETC inhibitors
179 phenformin and metformin.
180
181 **Dual inhibition of MCT1/4 in LCLs compromises OCR and NAD^+/NADH ratios, and induces**
182 **oxidative stress.** We next sought to explore the mechanisms responsible for the sensitivity of
183 LCLs to MCT inhibition. We performed Seahorse assays on LCLs treated with MCT1 and 4
184 inhibitors for 24 hours. As expected, dual MCT1/MCT4 inhibition, which induced lactate
185 accumulation in LCLs, significantly decreased extracellular acidification (**Fig. 5A**). Unexpectedly,
186 however, dual MCT1/4 inhibition significantly decreased oxygen consumption rates (OCR) after
187 just 24 hours of treatment indicating that these metabolic changes precede the growth arrest
188 observed at later time points (**Fig. 5B**). This effect was even more pronounced with the addition
189 of phenformin, which was expected given the unequivocal role of the ETC on mitochondrial
190 respiration (**Fig. 5B**).

191 The production of lactate during glycolysis is coupled with the regeneration of NAD^+ from
192 NADH. Therefore, we assessed the NAD^+/NADH ratio in MCT1/4 inhibited LCLs. We found that
193 treated cells had a significantly lower NAD^+/NADH ratio than control LCLs (**Fig. 5C**). Since
194 NAD^+/NADH ratios directly contribute to the redox state of the cell, we investigated whether
195 compromised NAD^+/NADH levels in MCT1/4-inhibited LCLs could be inducing oxidative stress.
196 Using the reactive oxygen species (ROS)-sensitive fluorescent DCFDA dye, we found that ROS
197 levels increased significantly upon MCT1/4 inhibition (**Fig. 5D**). Furthermore, metabolite tracing
198 experiments using heavy-labeled ^{13}C-glucose indicated that dual MCT1/4 inhibition increased the
199 fractional contribution of glucose in reduced and oxidized glutathione (**Fig. 5F,H**). Furthermore,
200 the marked decrease in glutathione pools by 72 hours post-treatment suggests an effort to
201 mitigate accumulating ROS levels through glutathione antioxidant activity (**Fig. 5G,I**)
202
203 **EBV+ and KSHV+ lymphoma cell lines are sensitive to dual MCT1/4 and ETC inhibitors.**
204 EBV is an etiologic factor in the development of B-cell lymphomas of the immune suppressed
205 such as HIV-associated diffuse large B-cell lymphomas (DLBCL) and post-transplant
206 lymphoproliferative disease (PTLD)(38–40). Therefore, we asked whether the novel approach of
207 dual MCT1/4 inhibition in EBV-immortalized LCLs could also be effective in EBV-positive
208 lymphoma cells. We treated the EBV+ AIDS-immunoblastic lymphoma cell line, IBL-1, which like
209 LCLs, expresses MCT1 and MCT4, with both MCT1/4 inhibitors (**Fig. 6C**). We observed a striking
210 diminution in growth, similar to the phenotype in LCLs (**Fig. 6A**). Consistently, we also observed
211 synergy between MCT1/4 antagonism and metformin as well as phenformin in IBL-1 cells, which
212 supports a novel therapeutic approach to EBV+ lymphomas (**Fig. 6A and 6B**).
213 Given the robustness of this strategy, we asked whether other viral lymphomas may be
214 susceptible to MCT antagonism and combination with metformin. Kaposi Sarcoma Herpesvirus
215 (KSHV) is a closely related oncogenic gamma herpesvirus to EBV and is the etiologic agent of
216 Kaposi Sarcoma as well as primary effusion lymphomas (PEL) in HIV-infected individuals. First,

217 we confirmed expression of MCT1 and MCT4 in the PEL cell lines BCBL-1, VG-1, and BCLM,
218 alongside IBL-1 and LCLs (**Fig. 6C**). Then, we investigated whether dual MCT1/4 inhibition could
219 impact PEL growth, especially when combined with metformin, as was true in LCLs and IBL-1
220 cells. Consistent with our observation in EBV-infected cells, we observed that dual inhibition of
221 MCT1 and 4 uniformly suppressed growth of KSHV-infected PEL cells. Furthermore, MCT1/4
222 antagonism also increased sensitivity of PEL cells to metformin-mediated growth inhibition,
223 thereby expanding the applicability of this strategy to KSHV+ lymphomas (**Fig. 6D**).

224 **DISCUSSION**

225 Epstein-Barr virus reorganizes B-cell metabolic pathways to promote immortalization as a
226 precursor to the development of lymphomas in the immune suppressed. We and others have
227 previously described a balanced upregulation of oxidative phosphorylation and glycolysis through
228 EBV-mediated B-cell outgrowth(3, 10). In order to maintain glycolytic flux during aerobic
229 glycolysis, EBV-infected B cells must upregulate lactate transporters. In this study, we identified
230 an EBNA2/c-Myc mediated upregulation of MCT1 that was important for supporting increased
231 glycolysis during the hyper-proliferative burst early after EBV infection. However, infected cells
232 became resistant to MCT1 antagonism between one- and two-weeks post infection and we
233 observed a strong upregulation of MCT4. This correlated with the switch in viral latency programs
234 in which the viral LMP1 protein promoted MCT4 expression. EBV-immortalized lymphoblastoid
235 cell lines were sensitive to the inhibition of both MCT1 and MCT4 with specific small molecule
236 antagonists, which led to their growth arrest due to a loss in the oxygen consumption rate, an
237 accumulation of both lactate and reactive oxygen species, and depletion of NAD^+ relative to
238 NADH. Importantly, MCT1/4 inhibition rendered LCLs vulnerable to the inhibition of the electron
239 transport chain with phenformin or metformin. This synergistic effect on LCLs was also manifested
240 in lymphoma cell lines harboring EBV and also a related oncogenic gammaherpesvirus, KSHV,
241 suggesting a novel strategy for targeting viral-induced cancers.

242 The role of monocarboxylate transporters (MCTs) has been well studied in cancer, but not
243 during viral infection. The metabolic requirements of both processes are similar with a goal of
244 ramping up anabolic processes to either promote proliferation or viral particle production. Latent
245 oncogenic herpesviruses are unique in that they express specific proteins and non-coding RNAs
246 that reprogram cellular transcription and metabolic pathways, with the goal of promoting viral
247 genome replication during host cell proliferation. For example, during KSHV lytic replication,
248 glycolysis is required for maximal virion production, while during latent infection, 10 out of the 12
249 microRNAs are sufficient to induce glycolysis, thereby contributing to infected cell growth (41, 42).
250 KSHV-associated PEL also display elevated aerobic glycolysis and fatty acid biosynthesis
251 compared to primary B cells, highlighting the importance of these pathways in KSHV-associated
252 tumors, and another parallel between KSHV infection and tumorigenesis(43),(44). Similarly, the
253 EBV oncoprotein LMP1 upregulates glucose import through NFκB signaling to promote cell
254 survival(8). Thus, EBV and KSHV coordinately activate their infected cells in a similar manner to
255 how cellular oncogenes cooperate to reprogram metabolism in cancer. While both EBV and
256 KSHV-associated lymphomas display increased extracellular acidification rates (ECAR) and
257 lactate export due to increased glycolysis, only a handful of studies have addressed lactate
258 transporters in these cancers(9, 45). In one study, MCT4 RNA was shown to be upregulated in
259 EBV-immortalized LCLs relative to mitogen-activated B cells and freshly EBV-infected B cells, but
260 mainly due to its association with the induction of hypoxia(9, 46). More indirectly, KSHV-infected
261 PEL chemoresistance to doxorubicin and paclitaxel has been linked to expression of the MCT1/4-
262 associated chaperone glycoprotein Emmprin, which is regulated by the KSHV-encoded latency-
263 associated nuclear antigen (LANA) in KSHV+ PEL cell lines (47),(48). Given the similarities
264 between EBV and KSHV-mediated reprogramming of host metabolism, and based on our
265 observation that KSHV+ PELs arrest upon treatment with both MCT1/4 inhibitors, it is therefore
266 possible that both viruses require and/or regulate MCT1/4-mediated lactate export in similar ways.
267 Future studies would need to elucidate whether MCT1/4-mediated lactate transport in KSHV+

268 lymphomas is intertwined with other aspects of metabolism like redox regulation and oxidative
269 stress mitigation, as is the case in EBV-immortalized LCLs.

270 During EBV infection, the EBV master transcriptional regulator EBNA2 can both directly
271 and indirectly influence host metabolic pathways such as one-carbon metabolism and fatty acid
272 biosynthesis through c-Myc(10, 49). We find that concomitant induction of MCT1 through c-Myc
273 is critical to support continued proliferation as lactate is generated through glycolysis.
274 Interestingly, we found that early-infected cells were exquisitely sensitive to MCT1 inhibition
275 through AZD3965 with low nanomolar (~1-10 nM) concentrations halting growth while in many
276 other tumor cell systems 250 nM is typically used. This suggests that MCT1-mediated lactate
277 export could be particularly important for B-cell growth in the absence of MCT4 – a gene
278 expression signature which has also been observed in germinal center B cells(32).

279 We were intrigued by the finding that EBV-infected B cells became resistant to MCT1
280 inhibition between one and two weeks after infection as this is the timeframe when infected cells
281 switch from proliferation driven by the viral EBNA proteins (latency IIb) to that of the EBNAs and
282 the LMPs (latency III)(5, 6). Given this relationship and the prior knowledge that MCT4 induction
283 could promote resistance to MCT1 antagonism, we interrogated MCT4 upregulation and
284 sensitivity to a novel MCT4 inhibitor. Our data support the upregulation of MCT4 by LMP1, which
285 is also supported by a published data set of LMP1 expression in DG75 cells(50). Moreover, that
286 study found that LMP1 targets dependent on the metabolic and DNA damage regulator, PARP1,
287 were largely enriched in HIF1α targets. In fact, their data using the PARP1 inhibitor olaparib
288 suggests that LMP1 induction of MCT4 was PARP1-dependent. These data also nicely dovetail
289 with that of a previous study supporting the stabilization of HIF1α and its targets in EBV-infected
290 cells supported a “pseudo-hypoxia” that appears to be induced by EBV(9).

291 The mechanism of growth arrest mediated by MCT1/4 antagonism involved a reduction in
292 the extracellular acidification rate due to the accumulation of lactate within cells, but surprisingly
293 also, a significant reduction in the oxygen consumption rate (OCR). Moreover, these effects were
294 observed within 24 hours following treatment, preceding cellular growth arrest which occurs
295 between 48-72 hours after treatment. We were intrigued by the significant decrease in OCR upon
296 dual MCT1/4 inhibition, given that previous reports describe increased OCR upon lactate export
297 inhibition as a means of compensating for reduced glycolysis with increased OXPHOS (20,
298 22),(51, 52). One possible explantion for this observed decrease in OCR could be due to the
299 altered redox balance via depleted NAD+/NADH, which could inhibiting NADH:ubiquinone
300 oxidoreductase activity in complex I of the ETC(53). Another possibility might be due to the
301 observed defect in *de novo* pyrimidine metabolism, as dihydroorotate dehydrogenase (DHODH)
302 function is directly linked to complex III activity(54). Either way, the reduction of OCR upon
303 selective MCT1/4 inhibition in LCLs points at a unique vulnerability that can be further exploited
304 for therapeutic benefit in EBV-driven lymphomas in combination with ETC inhibitors like
305 metformin. Recently, dual MCT1/4 inhibition using the anti-hypertensive drug syrosingopine was
306 found to be synthetically lethal with metformin in leukemia and breast cancer cell lines due to
307 depleted NAD^+/NADH ratios(30). Interestingly, we found that in LCLs, selective inhibition of both
308 MCT1 and MCT4 with AZD3965 and VB124 was sufficient to significantly deplete NAD^+/NADH
309 ratios, while addition of the metformin analog phenformin did not further deplete these ratios (not
310 shown). This therefore suggests an alternative mechanism of metformin/phenformin-induced
311 killing in MCT1/4-inhibited cancer cells, not directly related to NAD+/NADH metabolism.

312 The MCT1 inhibitor AZD3965 is currently in clinical trials for various lymphomas and solid
313 tumors(31). However, no such trials exist for MCT4, primarily due to the lack of MCT4-specific
314 inhibitors. While pan-MCT1/4 inhibitors do exist, these also target other metabolic pathways such
315 as the glycolytic enzyme enolase, and mitochondrial pyruvate transport in addition to MCT1 and

316 MCT4, which can produce adverse side effects(55, 56). Using the novel MCT4-specific inhibitor
317 VB124 as a tool compound, we were able to explore the therapeutic potential of MCT1/4-targeted
318 combination therapy in viral-associated lymhpomas. We recognize that pre-clinical testing of
319 AZD3965 and VB124 in primary cells and cell lines may be an incomplete representation of
320 lymphomagenesis *in vivo* as contributions from the tumor microenvironment are lacking.
321 However, EBV has a narrow host tropism and is unable to infect mice or other common small
322 animal models. Recent development of humanized mouse models of EBV infection will be useful
323 in assessing how metabolic pathways like MCT1/MCT4-mediated lactate transport contribue to
324 EBV-driven tumorigenesis *in vivo*(57).

325 **MATERIALS AND METHODS**

326 **Cell lines, culture conditions, and viruses**

327 Buffy coats were obtained from normal human donors through the Gulf Coast Regional
328 Blood Center (Houston, TX) and peripheral blood mononuclear cells (PBMCs) were isolated by
329 Ficoll Histopaque-1077 gradient (Sigma, H8889). B95-8 strain of Epstein-Barr virus was produced
330 from the B95-8 Z-HT cell line as previously described (52). Virus infections were performed in
331 bulk by adding 50 µL of filtered B95-8 supernatant to $1x10^6$ PBMCs.

332 All LCLs were kept in RPMI 1640 medium supplemented with 10% heat-inactivated fetal
333 bovine serum (Corning), 2 mM L-Glutamine, 100 U/ml penicillin, 100 µg/ml streptomycin
334 (Invitrogen), and 0.5 µg/mL Cyclosporine A (Sigma). The same conditions were used for the EBV−
335 germinal-center-derived B-cell lymphoma line BJAB (obtained from George Mosialos, Aristotle
336 University, Thessaloniki, Greece). Kaposi's sarcoma-associated herpesvirus-positive
337 (KSHV+)/EBV− primary effusion lymphoma (PEL) cell lines VG-1, BCLM, and BCBL1 were
338 provided by Dirk Dittmer (University of North Carolina [UNC], Chapel Hill, NC) or Bryan Cullen
339 (Duke University, Durham, NC) with permission from the original authors and kept in RPMI 1640

340 medium supplemented with 15% fetal bovine serum, 10 mM HEPES, 1 mM sodium pyruvate, and
341 0.05 mM β-mercaptoethanol (Sigma). The EBV-positive cell line derived from an AIDS
342 immunoblastic lymphoma, IBL-1, was kindly provided by Ethel Cesarman (Weill Cornell Medical
343 College, New York, NY) and kept in RPMI 1640 supplemented with 20% fetal bovine serum.
344 P493-6 cells (a kind gift of Dr. Georg Bornkamm, Helmholtz Zentrum München) were cultured in
345 RPMI 1640 supplemented with 10% tetracycline-free FBS (Hyclone SH30070), 1 μM β-Estradiol,
346 and 1 μg/mL Tetracycline. P493-6 cells were washed three times with β-Estradiol-free media, and
347 then cultured in the absence of β-Estradiol for 3 days to induce the EBNA2-OFF state. After
348 washing 3 times, the cells were then cultured again for 3 days upon reintroducing 1 uM β-
349 Estradiol, returning P493-6 cells to the EBNA2-ON state. All cells were cultured at 37°C in a
350 humidified incubator at 5% CO2.

351 **Flow cytometry and sorting**

352 To track proliferation in EBV-infected B cells, cells were stained with CellTrace Violet
353 (Invitrogen, C34557), a fluorescent proliferation-tracking dye. Cells were first washed in FACS
354 buffer (5% FBS in PBS), stained with the appropriate antibody for 30min-1hr at 4°C in the dark,
355 and then washed again before being analyzed on a BD FACS Canto II. Proliferating infected B
356 cells were sorted to a pure population of CD19+/CellTrace Violet on a MoFlo Astrios Cell Sorter
357 at the Duke Cancer Institute Flow Cytometry Shared Resource. Mouse anti-human CD19
358 antibody (Biolegend Cat# 152410) conjugated with APC was used as a surface B-cell marker in
359 flow cytometry.

360 **Cell Growth Assays**

361 LCLs were seeded at a density of $3x10^5$ cells/mL, and treated with either DMSO, AZD3965
362 (Cayman Chemicals), VB124 (a kind gift of Mark Parnell, Vettore LLC), phenformin (Cayman
363 Chemicals), or metformin (Cayman Chemicals) for one to four days. VB124 required

364 concentrations much higher than its IC50 (8.6 nM) in serum due to high(~99%) serum protein
365 binding common for carboxylic acids like VB124. Drug treatments were normalized across
366 conditions to contain 0.01% DMSO. Cell growth was assessed daily by either CellTiter Glo
367 (Promega) or counting by Trypan exclusion on an automated cell counter (Countess II,
368 ThermoFisher). Luminescence was measured using a microplate reader (Biotek Synergy HTX).

369 **Gene Expression Analysis**

370 Total RNA was isolated from cells by using a Qiagen RNeasy kit and then reverse transcribed to
371 generate cDNA with the High Capacity cDNA kit (Applied Biosystems). Quantitative PCR was
372 performed by using SYBR green (Quanta Biosciences) in an Applied Biosystems Step One Plus
373 instrument. Primer sets include MCT1 (**F:** GACCTTGTTGGACCCCAGAG,
374 **R**:AGCCGACCTAAAAGTGGTGG), MCT4 (**F:** AGGTCTACCTCACCACTGGG, **R**:
375 CACAGGAAGACAGGGCTACC.

376 **BrdU Staining**

377 Cell cycle progression was assessed by BrdU staining. Infected PBMCs treated with DMSO, Chk2
378 inhibitor II (EMD Millipore), or AZD3965 (Cayman Chemicals) cells were stained with CD19, and
379 pulsed with BrdU (BD Biosciences, Cat# 552598) for two hours following fixation and
380 permeabilization. Afterwards, cells were treated with a DNAse to expose BrdU-bound epitopes,
381 and stained wth a BrdU-fluorescent antibody as well as the total DNA and cell death marker 7-
382 AAD. Then, BrdU and 7-AAD fluorescence values were acquired on a flow cytometer (FACS
383 Canto II).

384 **Immunoblotting**

385 Cells were pelleted and washed in PBS, and then lysed in LDS Sample Buffer (NuPAGE) with
386 complete protease inhibitors. All protein lysates were run on NuPage 4–12% gradient gels

387 (LifeTechnology) and transferred to PVDF membrane (GE Healthcare). Membranes were blocked
388 in 5% milk in TBST and stained with primary antibody overnight at +4°C, followed by a wash and
389 staining with secondary HRP-conjugated antibody for 1 hour at room temperature. Antibodies
390 include MCT1 (Abcam, Cat# ab85021, 1:1000 dilution), MCT4 (Proteintech, Cat# 22787-1-AP,
391 1:1000 dilution), LMP1 (S12; gift from Elliot Kieff, Harvard Medical School), c-Myc (Santa Cruz
392 Biotechnology, SC-764), EBNA2 (PE2; gift from Elliot Kieff), MAGOH (Santa Cruz, SC-56724).
393 We use MAGOH as a loading control because it does not change in expression from resting B
394 cells through LCL outgrowth.

395 **Seahorse Analysis**

396 Extracellular acidification rate (ECAR) and oxygen consumption rate (OCR) were measured using
397 the Seahorse XFe96 extracellular flux analyzer (Agilent Technologies) Cell Energy Phenotype
398 Test. LCLs were attached to culture plates by using Cell-Tak (BD Bioscience). ECAR and OCR
399 were measured in Seahorse XF Base Medium supplemented with 1 mM pyruvate, 2 mM
400 glutamine, and 10 mM glucose (Sigma Aldrich). ECAR and OCR values were normalized to cell
401 number. For stress measurements, ECAR and OCR were measured over time after injection of
402 oligomycin and FCCP.

403 **^{13}C-glucose Tracing**

404 Glucose tracing experiments were performed using ^{13}C6-glucose (Cambridge Isotope
405 Laboratories Cat. CLM-1396-PK). LCLs were cultured in glucose-free RPMI supplemented with
406 10mM ^{13}C6-glucose and 10% dialyzed FBS, seeded at a density of 300,000 LCLs/mL and treated
407 with either DMSO or 1μM AZD3965 + 20μM VB124 for 48 or 72 hours. Then cells were harvested
408 and washed twice with ice-cold PBS, followed by metabolite extraction with ice-cold 80%
409 methanol in deionized water, and evaporation for approximately two hours. Dried metabolites
410 were reconstituted in 100 μL of a 50% acetonitrile(ACN) 50% dH20 solution. Samples were

411 vortexed and spun down for 10 min at 17,000g. 70 µL of the supernatant was then transferred to
412 HPLC glass vials. 10 µL of these metabolite solutions were injected per analysis. Samples were
413 run on a Vanquish (Thermo Scientific) UHPLC system with mobile phase A (20mM ammonium
414 carbonate, pH 9.7) and mobile phase B (100% ACN) at a flow rate of 150 µL/min on a SeQuant
415 ZIC-pHILIC Polymeric column (2.1 × 150 mm 5 µm, EMD Millipore) at 35°C. Separation was
416 achieved with a linear gradient from 20% A to 80% A in 20 min followed by a linear gradient from
417 80% A to 20% A from 20 min to 20.5 min. 20% A was then held from 20.5 min to 28 min. The
418 UHPLC was coupled to a Q-Exactive (Thermo Scientific) mass analyzer running in polarity
419 switching mode with spray-voltage=3.2kV, sheath-gas=40, aux-gas=15, sweep-gas=1, aux-gas-
420 temp=350°C, and capillary-temp=275°C. For both polarities mass scan settings were kept at full-
421 scan-range=(70-1000), ms1-resolution=70,000, max-injection-time=250ms, and AGC-
422 target=1E6. MS2 data was also collected from the top three most abundant singly-charged ions
423 in each scan with normalized-collision-energy=35. Each of the resulting ".RAW" files was then
424 centroided and converted into two ".mzXML" files (one for positive scans and one for negative
425 scans) using msconvert from ProteoWizard(58). These ".mzXML" files were imported into the
426 MZmine 2 software package(59). Ion chromatograms were generated from MS1 spectra via the
427 built-in Automated Data Analysis Pipeline (ADAP) chromatogram module and peaks were
428 detected via the ADAP wavelets algorithm(60). Peaks were aligned across all samples via the
429 Random sample consensus aligner module, gap-filled, and assigned identities using an exact
430 mass MS1(+/-15ppm) and retention time RT (+/-0.5min) search of our in-house MS1-RT
431 database. Peak boundaries and identifications were then further refined by manual curation.
432 Peaks were quantified by area under the curve integration and exported as CSV files. The peak
433 areas were additionally processed via the R package AccuCor to correct for natural isotope
434 abundance(61). Peak areas for each sample were normalized by the measured area of the
435 internal standard trifluoromethanesulfonate (present in the extraction buffer) and by the number
436 of cells present in the extracted sample.

437 **Lactate and NAD^+/NADH Measurements**

438 Intracellular and extracellular lactate concentrations were determined using the Lactate Glo
439 (Promega) assay kit. Briefly, cells were harvested and washed in ice cold PBS once, then
440 immediately inactivated with 0.6N HCl to halt metabolic activity and neutralized with 1M Tris base.
441 The resulting lysate was combined at a 1:1 ratio with the lactate detection reagent, and
442 luminescence measured a microplate reader. For intracellular lactate measurements involving
443 early-infection time points, PBMCs were first depleted for CD3+ T cells (RosetteSep™ Human
444 Granulocyte Depletion Cocktail), sorted to a pure population of CD19+ B cells on a MoFlo Astrios
445 Cell Sorter at the Duke Cancer Institute Flow Cytometry Shared Resource. Purified B cells were
446 either treated as indicated, or used as the starting cell population for time-course lactate
447 measurments. Mouse anti-human CD19 antibody (Biolegend Cat# 152410) conjugated with APC
448 was used as a surface B-cell marker in flow cytometry.

449 NAD^+/NADH ratios were measured using the NAD^+/NADH Glo assay (Promega)
450 according to the manufacturer's protocol. Briefly, harvested cells were washed in PBS, lysed with
451 Tris Base supplemented with 1% Dodecyl trimethylammonium bromide, treated with 0.4N HCl
452 (for NAD^+), and heated (for NADH) at 60°C for 15 min. Each sample was then added at a 1:1 ratio
453 with a luciferin detection reagent, and NAD^+ or NADH luminescence measured separately using
454 a BioTek Synergy™ 2 microplate reader.

455 **ROS Measurements**

456 ROS fluorescence was determined using the ROS-sensitive dye DCFDA (Cayman Chemicals Cat
457 #601520. Cells were pelleted and washed in the provided wash buffer, and then stained in 20μM
458 DCFDA for 1.5 hours at 37°C protected from light. Then, cells were washed once in the provided
459 wash buffer and FITC fluorescence measured in a flow cytometer. Pyocyanin (1mM) was used
460 as a positive control and N-acetylcysteine (300mM) as a negative control.

461 **ACKNOWLEDGMENTS**

462 This work was supported by National Institute of Health (NIH) grants R01-
463 CA140337 (to M.A.L.), T32GM007105-43, T32-CA009111 (to E.N.B.), T32CA009056 (to
464 J.C.), and R01 CA215185 (to H.R.C.) as well as RSG-16-111-01-MPC from the American
465 Cancer Society (to H.R.C.), the CDI Harry Winston Fellowship award (to J.C.), and the
466 St. Baldrick's Foundation Fellowship award (to J.C.). Additional funding came from the
467 Duke CFAR, and NIH-funded program (grant 5P30-Al064518).

468 The authors would like to thank Dr. Michael Cook, Nancy Martin, Lynn Martinek
469 and the Duke Cancer Institute Shared Flow Cytometry core facility for invaluable
470 assistance with flow cytometry and cell sorting. We would also like to thank Dr. Nancie
471 McIver and Amanda Nichols of the Duke Cellular Metabolism Analysis Core for their
472 guidance with the Seahorse XF anaysis. Finally, we would like to thank Ernst Schmid of
473 the UCLA Department of Biological Chemistry for assistance with mass spectrometry and
474 downstream analysis of isotopic tracing experiments.

475 **AUTHOR CONTRIBUTIONS**

476 M.A.L., E.N.B, J.E.M., J.M.C., H.R.C., and J.C. conceived and designed research
477 experiments. Specifically, M.A.L., J.E.M., and H.R.C. recognized that EBNA proteins may
478 regulate MCT1. J.E.M. with guidance from H.R.C. and J.C. initiated experiments on MCT1
479 regulation and function. J.E.M. trained E.N.B. in the laboratory with experimental
480 approaches on EBV-infection, drug treatments, and flow cytometry. E.N.B. and J.E.M.
481 performed buffy coat isolations from peripheral blood, EBV infections, and early-infection
482 treatment with AZD3965 and FACS analysis. E.N.B. performed all late-infection/LCL

483 treatments with MCT inhibitors, phenformin and metformin, lactate measurements,
484 Seahorse analysis, and metabolic assays. J.E.M. performed RNA-seq analysis, as well
485 as BrdU labeling. J.M.C. performed time-course qPCR experiments as well as all P493-
486 6 experiments. M.P. generously provided the MCT4 inhibitor VB124 and offered valuable
487 insight on experimental design of treatments in LCLs. J.C. and H.R.C. contributed to the
488 experimental design and execution of ^{13}C6-glucose tracing. E.N.B. and M.A.L. wrote and
489 all authors edited the manuscript.
490

491 **FIGURES AND FIGURE LEGENDS**

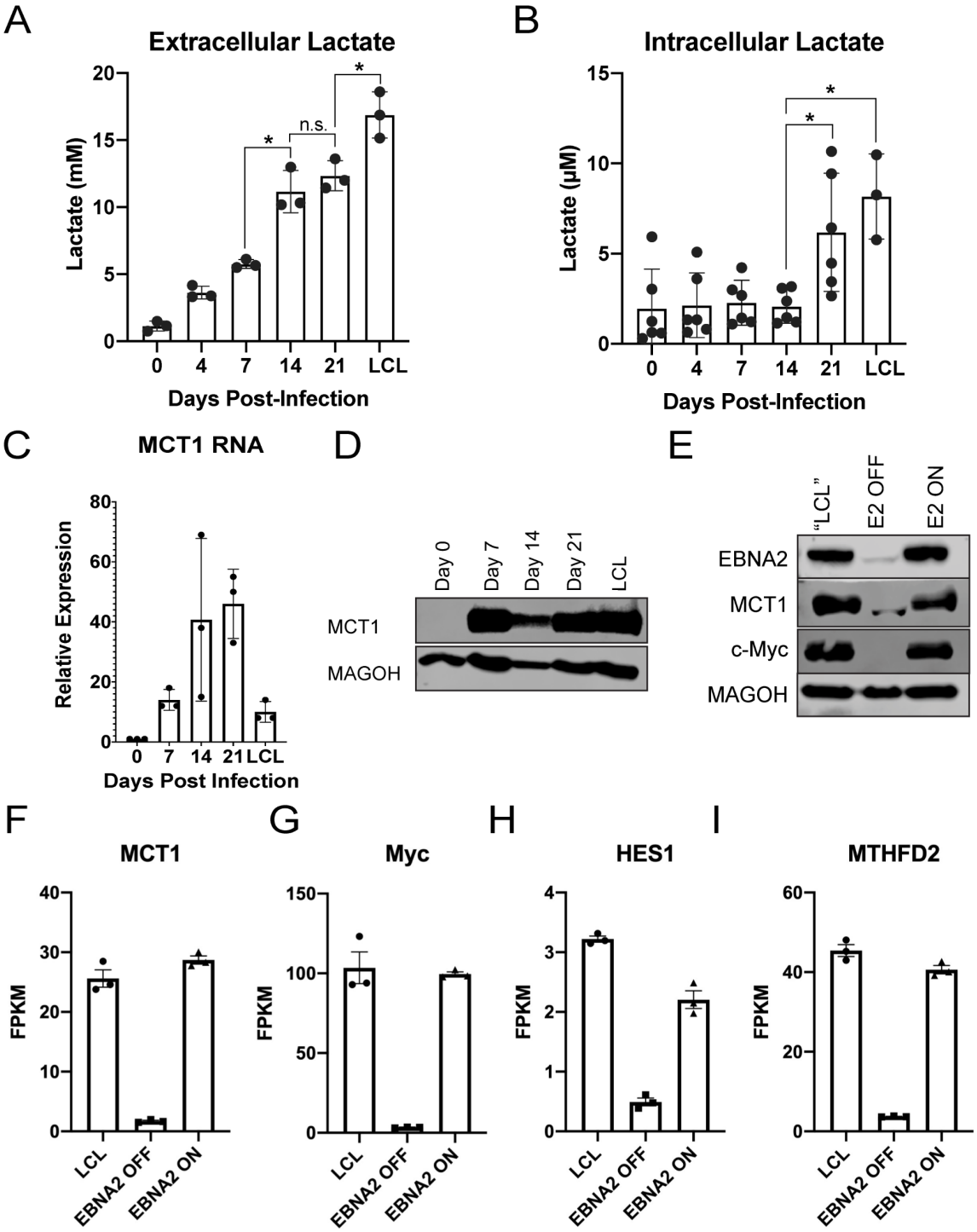

492

493 **Figure 1. EBV infection of human B cells leads to an increase in lactate transport**
494 **through MCT1.** ***A***. Extracellular (n=3) and ***B.*** Intracellular (n=6) lactate concentration
495 during EBV-infected B-cell immortalization. Extracellular concentration was obtained from
496 the supernatant of CD19+ isolated B cells at a concentration of $1x10^6$/mL and corrected
497 to cell-free growth medium lactate concentrations. Intracellular lactate concentration is
498 per 12,500 cells. ***C.*** MCT1 RNA (n=3) and ***D.*** Representative protein levels during EBV-
499 infected B-cell immortalization. MAGOH is a loading control used because the expression
500 of this gene is not changed upon B-cell outgrowth. ***E.*** Immunoblot of EBNA2, MCT1, and
501 c-Myc in P493-6 cells at the "LCL" state with stable EBNA2 expression, EBNA2 OFF in
502 the absence of β-estradiol, and EBNA2 ON with EBNA2 expression regained. ***F-I.*** RNA-
503 Seq data showing MCT1, c-Myc. HES1, and MTHFD2 expression in P493-6 B cells (n=3).
504 FPKM= Fragments Per Kilobase of transcript per Million mapped reads. Statistical
505 significance determined by paired t-test. *=p<0.05, **=p<0.01, ***=p<0.001.

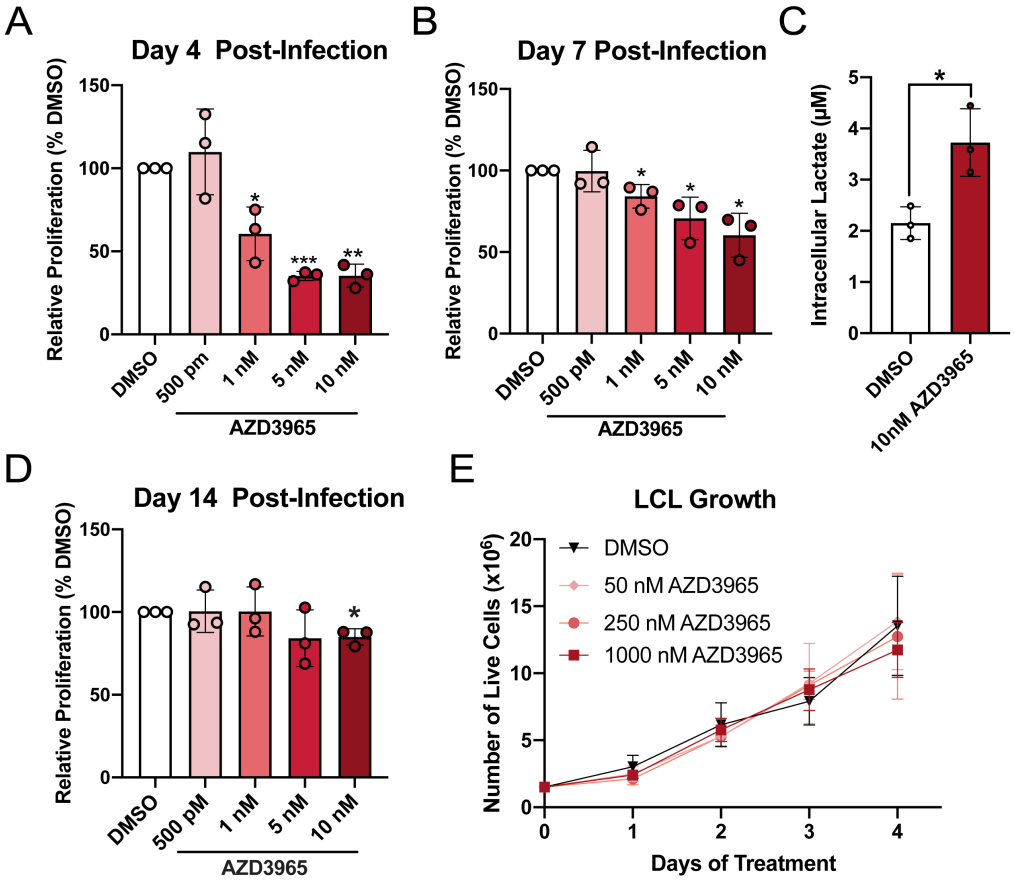

Figure 2. MCT1 inhibition leads to growth arrest and lactate buildup in early EBV-infected B cells. *A*. Bulk PBMCs (n=3) were treated with AZD3965 immediately following EBV infection, and CD19+ B-cell proliferation was determined by flow cytometry 4 days later. Cell counts were bead normalized. ***B.*** Bulk PBMCs (n=3) were treated 4 days post-infection, and CD19+ B-cell proliferation assessed by flow cytometry at 7 days post-infection. ***C.*** CD19-purified B cells (n=3) were treated at four days post-infection and intracellular lactate assessed three days later at seven days post-infection. ***D.*** Same as ***B***, except proliferation was assessed at 14 days post-infection. ***E.*** Growth curve of LCLs (n=3) treated with varying concentrations of AZD3965. LCL growth was determined by daily assessment of trypan blue exclusion. Statistical significance determined by paired t-test. *=p<0.05, **=p<0.01, ***=p<0.001.

518

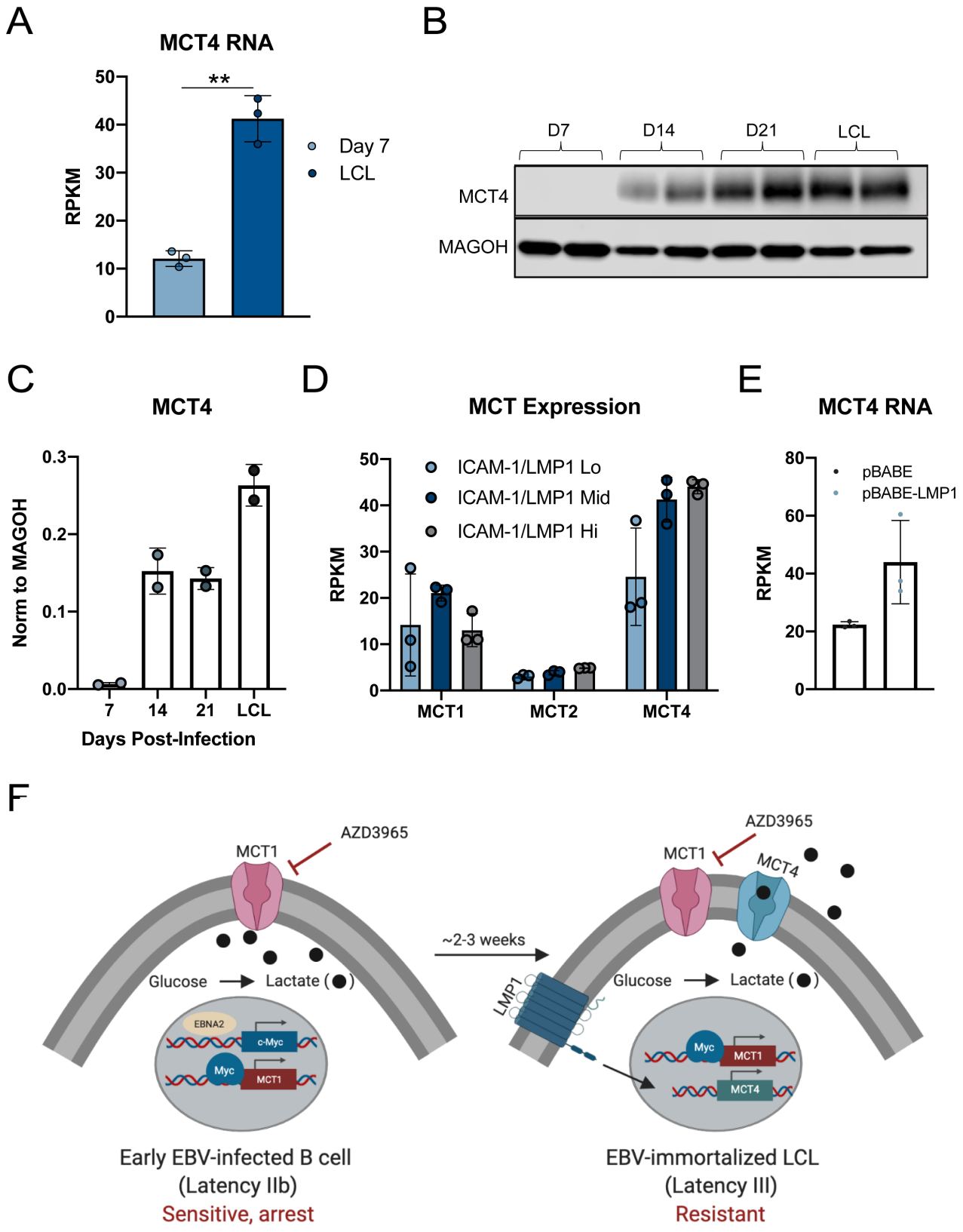
A
MCT4 RNA
**
RPKM
50
40
30
20
10
0
Day 7
LCL
B
D7
D14
D21
LCL
MCT4
MAGOH
C
MCT4
Norm to MAGOH
0.3
0.2
0.1
0.0
7
14
21
LCL
Days Post-Infection
D
MCT Expression
ICAM-1/LMP1 Lo
ICAM-1/LMP1 Mid
ICAM-1/LMP1 Hi
RPKM
50
40
30
20
10
0
MCT1
MCT2
MCT4
E
MCT4 RNA
pBABE
pBABE-LMP1
RPKM
80
60
40
20
0
F
AZD3965
MCT1
Glucose
Lactate
EBNA2
c-Myc
Myc
MCT1
~2-3 weeks
LMP1
AZD3965
MCT1
MCT4
Glucose
Lactate
Myc
MCT1
MCT4
Early EBV-infected B cell
(Latency IIb)
Sensitive, arrest
EBV-immortalized LCL
(Latency III)
Resistant

519

520 **Figure 3. EBV-infected B cells acquire resistance to MCT1 inhibition during B-cell**
521 **transformation due to MCT4 induction.** ***A.*** Queried RNA-Seq data of MCT4 expression
522 in EBV-infected B cells (n=3) at 7 days post-infection, and LCL(62). RPKM= Reads Per
523 Kilobase of transcript per Million mapped reads. ***B.*** Western blot of MCT4 in CD19+-
524 purified B cells during EBV-mediated B-cell immortalization. MAGOH= loading control. ***C.***
525 quantification of B (n=2). ***D.*** Monocarboxylate transporter (MCT) expression from RNA-
526 Seq of LCLs sorted by the LMP1 proxy, ICAM-1, status. ***E.*** Queried RNA-Seq data of
527 MCT4 expression in DG75 cells (n=3) transfected with LMP1. Statistical significance was
528 determined by paired t-test. *=p<0.05, **=p<0.01, ***=p<0.001. ***F***. Schematic representation
529 of MCT1 inhibitor sensitivity during EBV-mediated B lymphocyte immortalization.

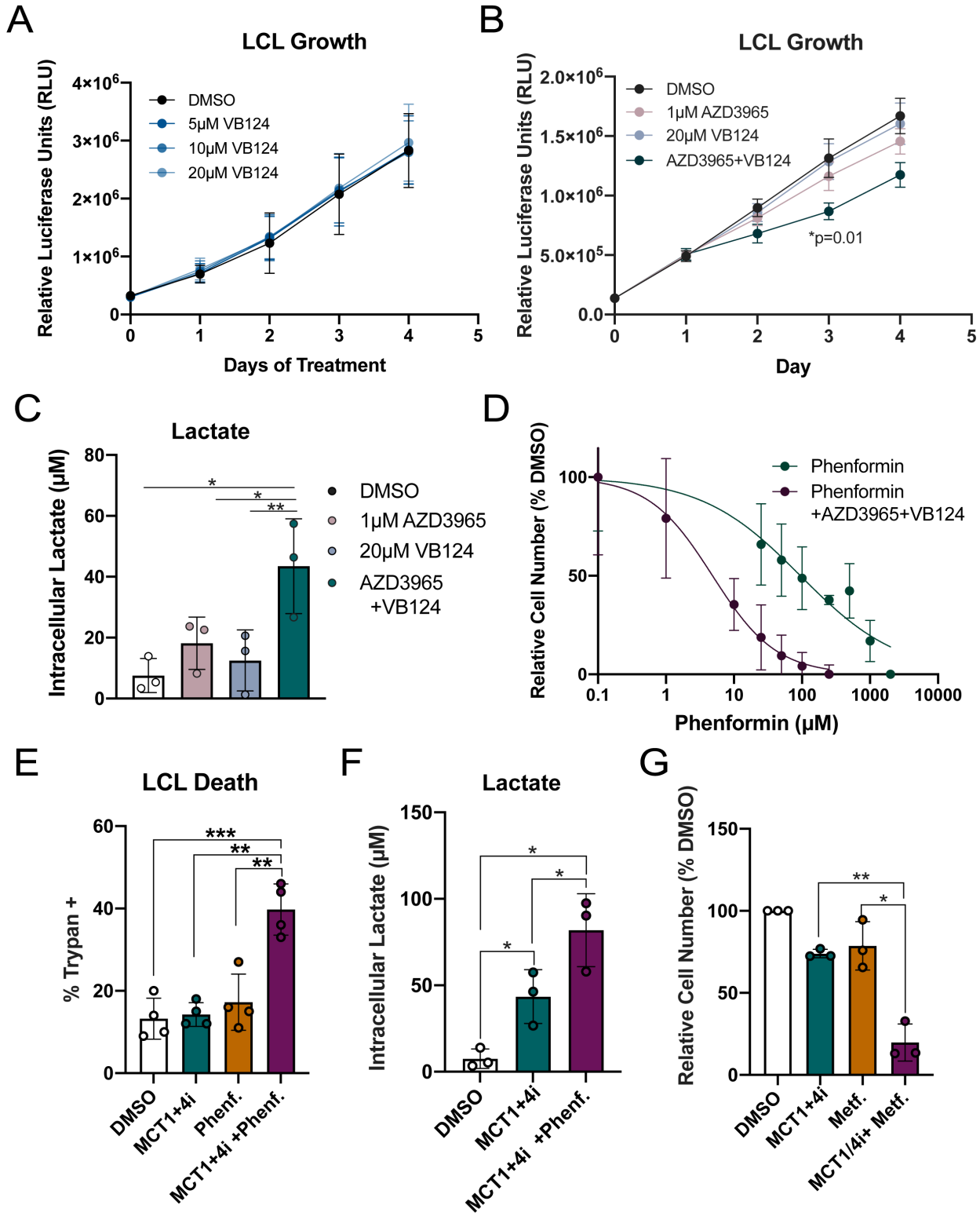

530

531 **Figure 4. Dual MCT1/4 inhibition sensitizes LCLs to killing by electron transport**

532 **chain (ETC) inhibitors.** ***A.*** Growth curve of LCLs (n=3) treated with varying

533 concentrations of VB124. Growth was determined by CellTiter Glo. ***B.*** Growth curve of
534 LCLs (n=3) treated with either DMSO, 1μM AZD3965, 20μM VB124, or 1μM AZD3965 +
535 20μM VB124. Growth was assessed as in A. ***C.*** Intracellular lactate concentration (per
536 12,500 cells), of LCLs (n=3) treated with either DMSO, 1μM AZD3965, 20μM VB124, or
537 1μM AZD3965 + 20μM VB124. ***D.*** Phenformin IC50 curve. Generated 72h after treatment
538 of LCLs (n=3) with either phenformin or 1μM AZD3965 + 20μM VB124. Relative cell
539 number was determined by CellTiter Glo luminescence. Values were normalized to
540 DMSO to obtain %DMSO. ***E.*** LCL death, as determined by trypan blue staining after 72h
541 of treatment. n=3. MCT1+4i= 1μM AZD3965 + 20μM VB124, Phenf. = 10μM Phenformin
542 ***F.*** Intracellular lactate concentration (per 12,500 cells), of LCLs treated for 3 days ***G.***
543 Relative LCL number as determined by CellTiter Glo, 72h after treatment. n=3. MCT1+4i=
544 1μM AZD3965 + 20μM VB124, Metf. = 2mM Metformin. Statistical significance was
545 determined by paired t-test. ***H.*** LCL death, based on trypan blue positivity, following 72h
546 of treatment. n=3. *=p<0.05, **=p<0.01, ***=p<0.001.

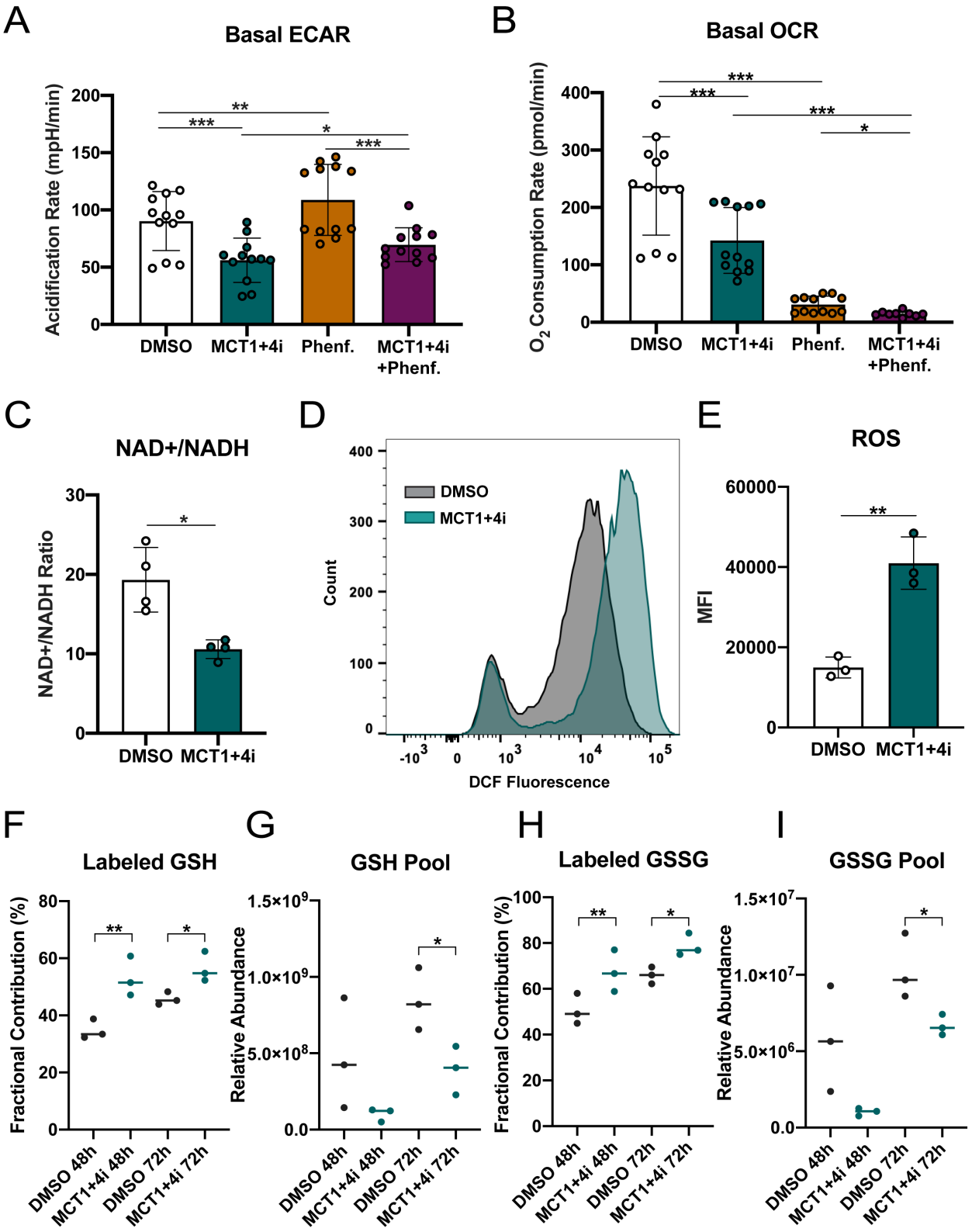
A
Basal ECAR
Acidification Rate (mpH/min)
200
150
100
50
0
**
***
*
***
DMSO
MCT1+4i
Phenf.
MCT1+4i +Phenf.
B
Basal OCR
O2 Consumption Rate (pmol/min)
400
300
200
100
0
***
***
***
*
DMSO
MCT1+4i
Phenf.
MCT1+4i +Phenf.
C
NAD+/NADH
NAD+/NADH Ratio
30
20
10
0
*
DMSO
MCT1+4i
D
Count
400
300
200
100
0
DMSO
MCT1+4i
-10^3
0
10^3
10^4
10^5
DCF Fluorescence
E
ROS
MFI
60000
40000
20000
0
**
DMSO
MCT1+4i
F
Labeled GSH
Fractional Contribution (%)
80
60
40
20
0
**
*
DMSO 48h
MCT1+4i 48h
DMSO 72h
MCT1+4i 72h
G
GSH Pool
Relative Abundance
1.5×10^9
1.0×10^9
5.0×10^8
0.0
*
DMSO 48h
MCT1+4i 48h
DMSO 72h
MCT1+4i 72h
H
Labeled GSSG
Fractional Contribution (%)
100
80
60
40
20
0
**
*
DMSO 48h
MCT1+4i 48h
DMSO 72h
MCT1+4i 72h
I
GSSG Pool
Relative Abundance
1.5×10^7
1.0×10^7
5.0×10^6
0.0
*
DMSO 48h
MCT1+4i 48h
DMSO 72h
MCT1+4i 72h

547

548 **Figure 5. Dual inhibition on MCT1/4 in LCLs compromises OCR and NAD/NADH**
549 **ratios and induces oxidative stress.** ***A.*** Seahorse assay showing extracellular
550 acidification rate (ECAR) and ***B.*** Oxygen consumption rate (OCR) of LCLs (n=4) in
551 triplicate. MCT1+4i= 1μM AZD3965 + 20μM VB124. Phenf. = 10μM Phenformin. ***C.***
552 NAD^+/NADH ratio of LCLs (n=4) treated for 48h ***D.*** Fluorescence-activated cell sorting
553 (FACS) histograms of treated LCLs (n=3) stained with 2',7'-dichlorodihydrofluorescein
554 diacetate (H_2-DCFDA). ***E.*** Mean fluorescence intensity (MFI) of D. ***F-I.*** Metabolic analysis
555 with ^{13}C-6-glucose tracing of reduced (GSH) or oxidized (GSSG) glutathione in LCLs
556 (n=3) treated with either DMSO or MCT1+MCT4 inhibitors for 48h or 72h. Cells were
557 cultured in the presence of ^{13}C6-labeled glucose-supplemented RPMI medium. Fractional
558 contribution= % heavy-labeled GSH or GSSG relative to pool size. Pool= Relative
559 abundance of GSH or GSSH in sample, as determined by LC-MS. Statistical significance
560 was determined by paired t-test. *=p<0.05, **=p<0.01, ***=p<0.001.

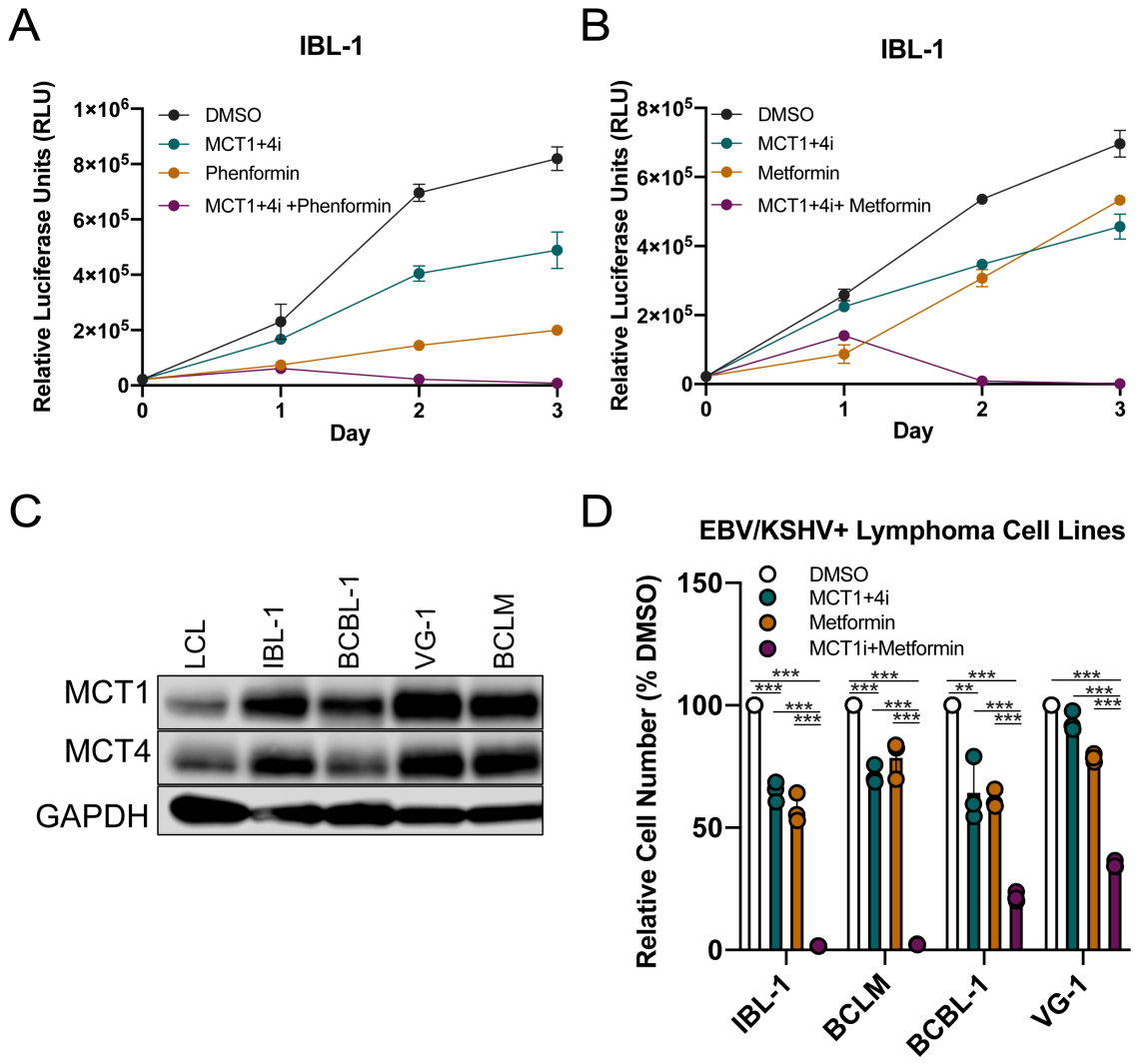

Figure 6. EBV+ and KSHV+ lymphoma cell lines are sensitized to killing by metformin upon dual MCT1/4 inhibition. *A, B.* Growth over time of the EBV+ AIDS immunoblastic lymphoma cell line IBL-1 (n=3), in the presence of both MCT1/4 inhibitors, and ETC inhibitors metformin and phenformin. MCT1+4i= 1μM AZD3965 + 20μM VB124. Phenformin= 100μM Metformin= 2mM. CellTiter Glo luminescence was used as proxy for cell growth. ***C***. Immunoblot of MCT1 and MCT4 in EBV+ or KSHV+ primary effusion lymphoma (PEL) cell lines, compared to EBV-immortalized LCLs. IBL-1= EBV+, KSHV- AIDS immunoblastic lymphoma, BCBL-1= EBV-, KSHV+ PEL, VG-1= EBV-, KSHV+ PEL,

570 BCLM= EBV-, KSHV+ PEL. GAPDH= loading control. ***D.*** Relative cell count of
571 EBV+/KSHV+ lymphoma cell lines (n=3) 48h after treatment. Statistical significance was
572 determined by multiple t-test. *=p<0.05, **=p<0.01, ***=p<0.001.

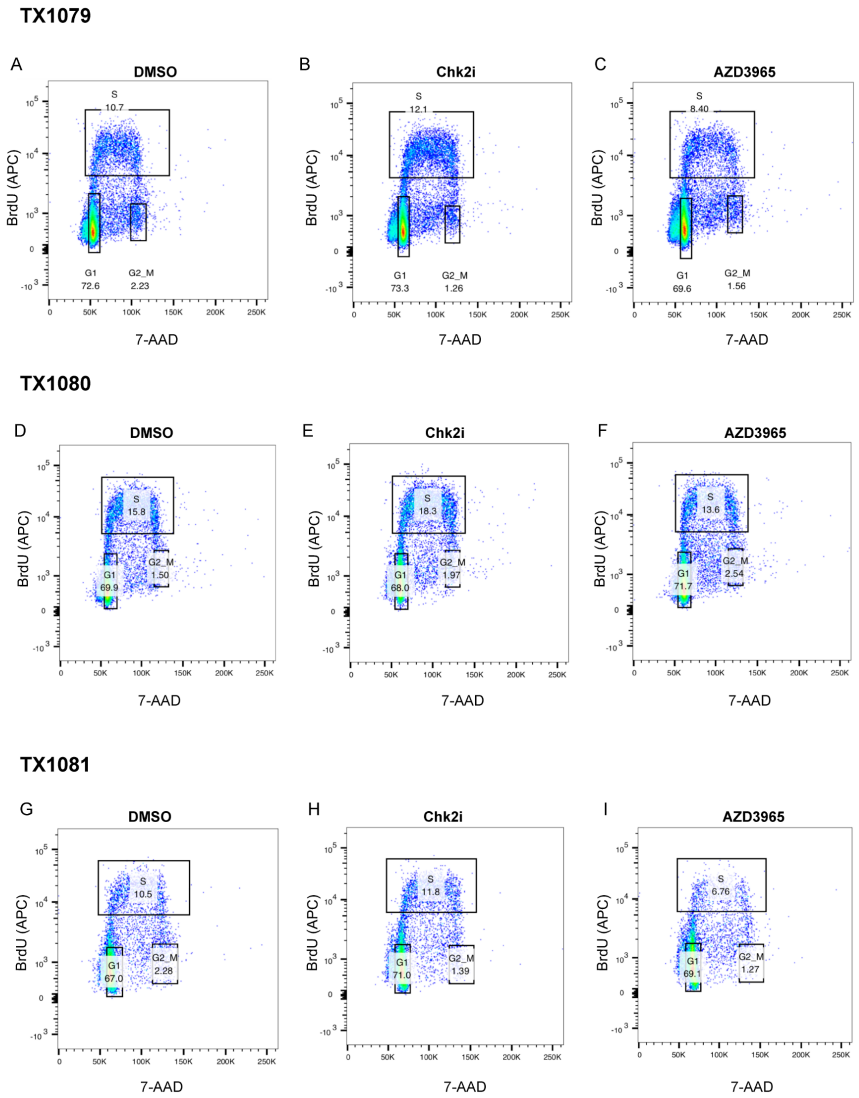

573

574 **Supplementary Figure 1. MCT1 inhibition in early EBV-infected B cells leads to a G1/S-**
575 **phase growth arrest, and not cell death.** ***A-I.*** Three PBMC donors were treated with either
576 DMSO, 5μM Chk2 inhibitor II, or 250nM AZD3965 for 48h. After 48h, cells were pulsed with BrdU
577 for 2h, and cell cycle progression assessed by flow cytometry. Chk2i = positive proliferation
578 control.

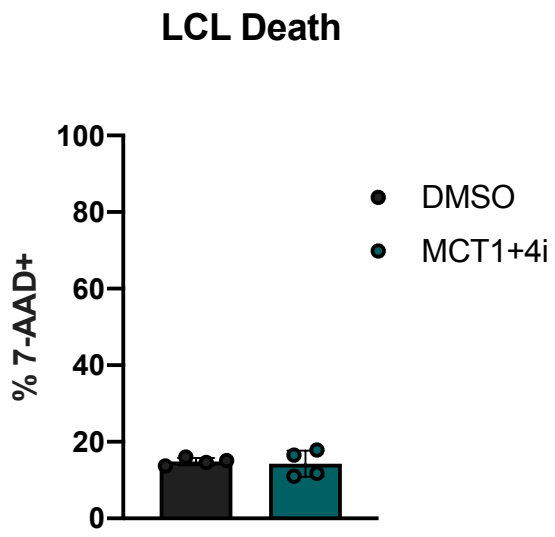

579

580 **Supplementary Figure 2. Dual MCT1/4 inhibition in LCLs does not result in cell death.** Two
581 LCL donors were treated in duplicate (n=4) with either DMSO or 1μM AZD3965 + 20μM VB124
582 for 72h, and 7-AAD positivity was assessed via fluorescence-activated cell sorting (FACS).

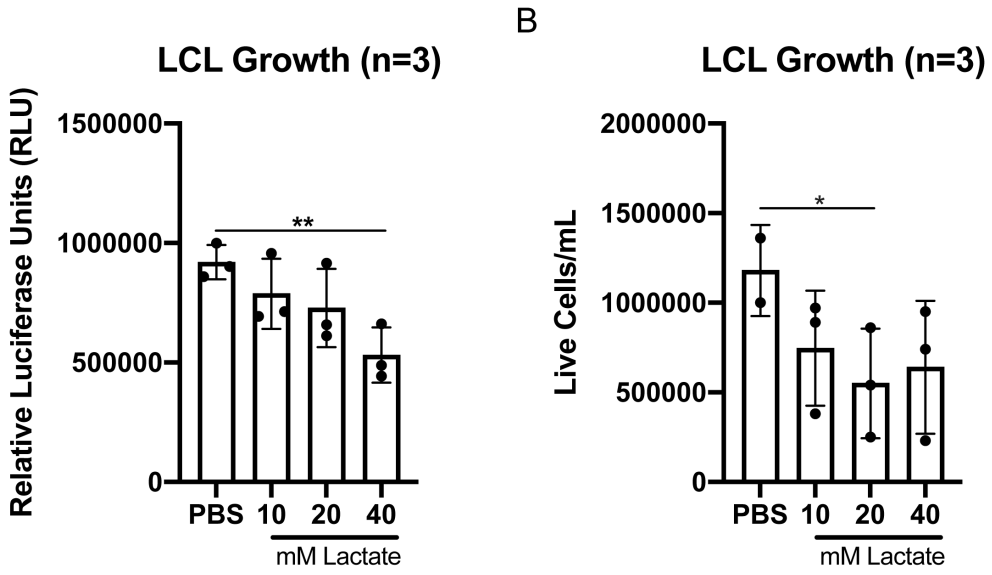

583

584 **Supplementary Figure 3. Exogenous L-lactate treatment in LCLs leads to growth arrest.**
585 LCLs were treated for 72h with varying concentrations of L-lactate. Growth was assessed by
586 either CellTiter Glo (***A***) or trypan blue exlusion counting (***B***). Statistical significance was
587 determined by paired t-test. *=p<0.05, **=p<0.01.

588 **REFERENCES**

589 1. G. J. Babcock, L. L. Decker, M. Volk, D. A. Thorley-Lawson, EBV Persistence in Memory B
590 Cells In Vivo. *Immunity* **9**, 395–404 (1998).

591 2. P. A. Nikitin, *et al.*, An ATM/Chk2-mediated DNA damage-responsive signaling pathway
592 suppresses Epstein-Barr virus transformation of primary human B cells. *Cell Host Microbe*
593 **8**, 510–522 (2010).

594 3. K. McFadden, *et al.*, Metabolic stress is a barrier to Epstein–Barr virus-mediated B-cell
595 immortalization. *Proc. Natl. Acad. Sci.* **113**, E782–E790 (2016).

596 4. C. Shannon-Lowe, A. B. Rickinson, A. I. Bell, Epstein–Barr virus-associated lymphomas.
597 *Philos. Trans. R. Soc. B Biol. Sci.* **372** (2017).

598 5. A. M. Price, M. A. Luftig, To Be or Not IIb: A Multi-Step Process for Epstein-Barr Virus Latency
599 Establishment and Consequences for B Cell Tumorigenesis. *PLOS Pathog.* **11**, e1004656
600 (2015).

601 6. J. E. Messinger, J. Dai, L. J. Stanland, A. M. Price, M. A. Luftig, Identification of Host
602 Biomarkers of Epstein-Barr Virus Latency IIb and Latency III. *mBio* **10** (2019).

603 7. P. A. Nikitin, A. M. Price, K. McFadden, C. M. Yan, M. A. Luftig, Mitogen-induced B-cell
604 proliferation activates Chk2-dependent G1/S cell cycle arrest. *PloS One* **9**, e87299 (2014).

605 8. T. Sommermann, K. O'Neill, D. R. Plas, E. Cahir-McFarland, IKKβ and NFκB transcription
606 govern lymphoma cell survival through AKT-induced plasma membrane trafficking of
607 GLUT1. *Cancer Res.* **71**, 7291–7300 (2011).

608 9. S. Darekar, *et al.*, Epstein-Barr Virus Immortalization of Human B-Cells Leads to Stabilization
609 of Hypoxia-Induced Factor 1 Alpha, Congruent with the Warburg Effect. *PLoS ONE* **7**
610 (2012).

611 10. L. W. Wang, *et al.*, Epstein-Barr-Virus-Induced One-Carbon Metabolism Drives B Cell
612 Transformation. *Cell Metab.* **30**, 539-555.e11 (2019).

613 11. M. Sola-Penna, Metabolic regulation by lactate. *IUBMB Life* **60**, 605–608 (2008).

614 12. S. Sun, H. Li, J. Chen, Q. Qian, Lactic Acid: No Longer an Inert and End-Product of Glycolysis.
615 *Physiology* **32**, 453–463 (2017).

616 13. J. Chiche, *et al.*, In vivo pH in metabolic-defective Ras-transformed fibroblast tumors: Key role
617 of the monocarboxylate transporter, MCT4, for inducing an alkaline intracellular pH. *Int. J.*
618 *Cancer* **130**, 1511–1520 (2012).

619 14. A. P. Halestrap, N. T. Price, The proton-linked monocarboxylate transporter (MCT) family:
620 structure, function and regulation. *Biochem. J.* **343 Pt 2**, 281–299 (1999).

621 15. A. Ritzhaupt, I. S. Wood, A. Ellis, K. B. Hosie, S. P. Shirazi-Beechey, Identification and
622 characterization of a monocarboxylate transporter (MCT1) in pig and human colon: its
623 potential to transport L-lactate as well as butyrate. *J. Physiol.* **513 (Pt 3)**, 719–732 (1998).

624 16. W. N. Fishbein, N. Merezhinskaya, J. W. Foellmer, Relative distribution of three major lactate
625 transporters in frozen human tissues and their localization in unfixed skeletal muscle.
626 *Muscle Nerve* **26**, 101–112 (2002).

627 17. B. Deuticke, Monocarboxylate transport in erythrocytes. *J. Membr. Biol.* **70**, 89–103 (1982).

628 18. N. T. Price, V. N. Jackson, A. P. Halestrap, Cloning and sequencing of four new mammalian
629 monocarboxylate transporter (MCT) homologues confirms the existence of a transporter
630 family with an ancient past. *Biochem. J.* **329 (Pt 2)**, 321–328 (1998).

631 19. K. S. Dimmer, B. Friedrich, F. Lang, J. W. Deitmer, S. Bröer, The low-affinity monocarboxylate
632 transporter MCT4 is adapted to the export of lactate in highly glycolytic cells. *Biochem. J.*
633 **350 Pt 1**, 219–227 (2000).

634 20. C. S. Hong, *et al.*, MCT1 modulates cancer cell pyruvate export and growth of tumors that co-
635 express MCT1 and MCT4. *Cell Rep.* **14**, 1590–1601 (2016).

636 21. J. R. Doherty, J. L. Cleveland, Targeting lactate metabolism for cancer therapeutics. *J. Clin.*
637 *Invest.* **123**, 3685–3692 (2013).

638 22. J. R. Doherty, *et al.*, Blocking Lactate Export by Inhibiting the Myc Target MCT1 Disables
639 Glycolysis and Glutathione Synthesis. *Cancer Res.* **74**, 908–920 (2014).

640 23. D. M. Voss, *et al.*, Disruption of the monocarboxylate transporter-4-basigin interaction inhibits
641 the hypoxic response, proliferation, and tumor progression. *Sci. Rep.* **7** (2017).

642 24. C. Juel, Lactate-proton cotransport in skeletal muscle. *Physiol. Rev.* **77**, 321–358 (1997).

643 25. A. Bonen, S. K. Baker, H. Hatta, Lactate transport and lactate transporters in skeletal muscle.
644 *Can. J. Appl. Physiol. Rev. Can. Physiol. Appl.* **22**, 531–552 (1997).

645 26. P. D. Bosshart, D. Kalbermatter, S. Bonetti, D. Fotiadis, Mechanistic basis of L-lactate
646 transport in the SLC16 solute carrier family. *Nat. Commun.* **10** (2019).

647 27. S. Hui, *et al.*, Glucose feeds the TCA cycle via circulating lactate. *Nature* **551**, 115–118 (2017).

648 28. D. Whitaker-Menezes, *et al.*, Evidence for a stromal-epithelial “lactate shuttle” in human
649 tumors. *Cell Cycle* **10**, 1772–1783 (2011).

650 29. M. Beloueche-Babari, *et al.*, MCT1 inhibitor AZD3965 increases mitochondrial metabolism,
651 facilitating combination therapy and non-invasive magnetic resonance spectroscopy.
652 *Cancer Res.* **77**, 5913–5924 (2017).

653 30. D. Benjamin, *et al.*, Dual Inhibition of the Lactate Transporters MCT1 and MCT4 Is Synthetic
654 Lethal with Metformin due to NAD+ Depletion in Cancer Cells. *Cell Rep.* **25**, 3047-3058.e4
655 (2018).

656 31. , A Phase I Trial of AZD3965 in Patients With Advanced Cancer - Full Text View -
657 ClinicalTrials.gov (April 14, 2020).

658 32. N. J. Curtis, *et al.*, Pre-clinical pharmacology of AZD3965, a selective inhibitor of MCT1:
659 DLBCL, NHL and Burkitt's lymphoma anti-tumor activity. *Oncotarget* **8**, 69219–69236
660 (2017).

661 33. C. Kaiser, *et al.*, The Proto-Oncogene c-myc Is a Direct Target Gene of Epstein-Barr Virus
662 Nuclear Antigen 2. *J. Virol.* **73**, 4481–4484 (1999).

663 34. A. Pajic, *et al.*, Cell cycle activation by c-myc in a Burkitt lymphoma model cell line. *Int. J.*
664 *Cancer* **87**, 787–793 (2000).

665 35. S. Maier, *et al.*, Cellular Target Genes of Epstein-Barr Virus Nuclear Antigen 2. *J. Virol.* **80**,
666 9761–9771 (2006).

667 36. 36. Ahmad A. Cluntun, *et al*., The Pyruvate-Lactate Axis Modulates Cardiac Hypertrophy and
668 Heart Failure. *Cell Metab*. (2020).

669 37. I. Marchiq, R. Le Floch, D. Roux, M.-P. Simon, J. Pouyssegur, Genetic disruption of lactate/H+
670 symporters (MCTs) and their subunit CD147/BASIGIN sensitizes glycolytic tumor cells to
671 phenformin. *Cancer Res.* **75**, 171–180 (2015).

672 38. M. Bibas, A. Antinori, EBV and HIV-Related Lymphoma. *Mediterr. J. Hematol. Infect. Dis.* **1**
673 (2009).

674 39. S. A. Rezk, L. M. Weiss, Epstein-Barr virus-associated lymphoproliferative disorders. *Hum.*
675 *Pathol.* **38**, 1293–1304 (2007).

676 40. V. R. Dharnidharka, *et al.*, Post-transplant lymphoproliferative disorders. *Nat. Rev. Dis. Primer*
677 **2**, 15088 (2016).

678 41. E. L. Sanchez, *et al.*, Glycolysis, Glutaminolysis, and Fatty Acid Synthesis Are Required for
679 Distinct Stages of Kaposi's Sarcoma-Associated Herpesvirus Lytic Replication. *J. Virol.* **91**
680 (2017).

681 42. M. Lagunoff, Activation of cellular metabolism during latent Kaposi's Sarcoma herpesvirus
682 infection. *Curr. Opin. Virol.* **19**, 45–49 (2016).

683 43. A. P. Bhatt, *et al.*, Dysregulation of fatty acid synthesis and glycolysis in non-Hodgkin
684 lymphoma. *Proc. Natl. Acad. Sci.* **109**, 11818–11823 (2012).

685 44. E. Currie, A. Schulze, R. Zechner, T. C. Walther, R. V. Farese, Cellular fatty acid metabolism
686 and cancer. *Cell Metab.* **18**, 153–161 (2013).

687 45. T. Delgado, *et al.*, Induction of the Warburg effect by Kaposi's sarcoma herpesvirus is required
688 for the maintenance of latently infected endothelial cells. *Proc. Natl. Acad. Sci. U. S. A.*
689 **107**, 10696–10701 (2010).

690 46. M. S. Ullah, A. J. Davies, A. P. Halestrap, The Plasma Membrane Lactate Transporter MCT4,
691 but Not MCT1, Is Up-regulated by Hypoxia through a HIF-1α-dependent Mechanism. *J.*
692 *Biol. Chem.* **281**, 9030–9037 (2006).

693 47. L. Dai, *et al.*, Emmprin and KSHV: New partners in viral cancer pathogenesis. *Cancer Lett.*
694 **337**, 161–166 (2013).

695 48. Z. Qin, L. Dai, M. G. Slomiany, B. P. Toole, C. Parsons, Direct activation of emmprin and
696 associated pathogenesis by an oncogenic herpesvirus. *Cancer Res.* **70**, 3884–3889
697 (2010).

698 49. L. W. Wang, *et al.*, Epstein-Barr virus subverts mevalonate and fatty acid pathways to promote
699 infected B-cell proliferation and survival. *PLoS Pathog.* **15** (2019).

700 50. M. Hulse, *et al.*, Poly(ADP-ribose) polymerase 1 is necessary for coactivating hypoxia-
701 inducible factor-1-dependent gene expression by Epstein-Barr virus latent membrane
702 protein 1. *PLoS Pathog.* **14**, e1007394 (2018).

703 51. J. Xie, *et al.*, Beyond Warburg effect – dual metabolic nature of cancer cells. *Sci. Rep.* **4**
704 (2014).

705 52. H. Wu, M. Ying, X. Hu, Lactic acidosis switches cancer cells from aerobic glycolysis back to
706 dominant oxidative phosphorylation. *Oncotarget* **7**, 40621–40629 (2016).

707 53. W. Ying, NAD+/NADH and NADP+/NADPH in Cellular Functions and Cell Death: Regulation
708 and Biological Consequences. *Antioxid. Redox Signal.* **10**, 179–206 (2007).

709 54. A. A. Khutornenko, *et al.*, Pyrimidine biosynthesis links mitochondrial respiration to the p53
710 pathway. *Proc. Natl. Acad. Sci.* **107**, 12828–12833 (2010).

711 55. S. J. Park, *et al.*, An overview of MCT1 and MCT4 in GBM: small molecule transporters with
712 large implications. *Am. J. Cancer Res.* **8**, 1967–1976 (2018).

713 56. D. Benjamin, *et al.*, Syrosingopine sensitizes cancer cells to killing by metformin. *Sci. Adv.* **2**
714 (2016).

715 57. M. Islas-Ohlmayer, *et al.*, Experimental Infection of NOD/SCID Mice Reconstituted with
716 Human CD34+ Cells with Epstein-Barr Virus. *J. Virol.* **78**, 13891–13900 (2004).

717 58. M. C. Chambers, *et al.*, A cross-platform toolkit for mass spectrometry and proteomics. *Nat.*
718 *Biotechnol.* **30**, 918–920 (2012).

719 59. T. Pluskal, S. Castillo, A. Villar-Briones, M. Orešič, MZmine 2: Modular framework for
720 processing, visualizing, and analyzing mass spectrometry-based molecular profile data.
721 *BMC Bioinformatics* **11**, 395 (2010).

722 60. O. D. Myers, S. J. Sumner, S. Li, S. Barnes, X. Du, One Step Forward for Reducing False
723 Positive and False Negative Compound Identifications from Mass Spectrometry
724 Metabolomics Data: New Algorithms for Constructing Extracted Ion Chromatograms and
725 Detecting Chromatographic Peaks. *Anal. Chem.* **89**, 8696–8703 (2017).

726 61. X. Su, W. Lu, J. D. Rabinowitz, Metabolite Spectral Accuracy on Orbitraps. *Anal. Chem.* **89**,
727 5940–5948 (2017).

728 62. A. M. Price, J. E. Messinger, M. A. Luftig, c-Myc Represses Transcription of Epstein-Barr
729 Virus Latent Membrane Protein 1 Early after Primary B Cell Infection. *J. Virol.* **92**, e01178-
730 17 (2018).

731